RESEARCH ARTICLE

CRISPR-Cas12a technology for the assembly and regulation of biomaterials

Chenguang Bi*, Xiaodong Zhan, Jie Hu

School of Public Administration, Chongqing Vocational College of Transportation, Chongqing, China.

Received: November 14, 2025; **accepted:** March 25, 2026.

Smart biomaterials constitute a pioneering domain within biomedicine. However, conventional response mechanisms that depend on physical or chemical stimuli inherently face limitations concerning specificity and programmability. To achieve precise control over the assembly and functionality of biomaterials at the nucleic acid sequence level, a dual-function regulatory platform was developed in this research, leveraging the CRISPR-Cas12a system. In terms of assembly, Cas12a cis-cleavage of bridged DNA generated directional sticky ends, and a four-armed PEG-DNA precursor was programmably cross-linked to construct a hydrogel. A dsDNA activator was then added to trigger trans-cleavage of pre-loaded Cas12a/crRNA (CRISPR RNA), degrading the gel network as needed. The results showed that this proposed system could efficiently assemble a mechanically tunable elastic hydrogel within 25 minutes. Under the triggering of a perfectly matched DNA activator, the gel rapidly disintegrated within 2 hours with a storage modulus decay rate as high as 96.814%, while, for sequences containing only a single base mismatch, the modulus decay rate was less than 5%. This material system exhibited excellent biocompatibility with the viability of human umbilical vein endothelial cells encapsulated within it remaining above 92.837% after five days of three-dimensional culture. This research successfully extended the molecular recognition and catalytic capabilities of CRISPR-Cas12a to the field of materials science, establishing a new approach for the design, assembly, and dynamic regulation of intelligent biomaterials based on nucleic acid sequence logic.

Keywords: CRISPR-Cas12a; biomaterials; molecular assembly; smart response; hydrogel.

***Corresponding author:** Chenguang Bi, School of Public Administration, Chongqing Vocational College of Transportation, Chongqing 402247, China. Email: bichenguang2017@163.com.

Introduction

As a pivotal frontier in biomedical engineering, intelligent biomaterials have witnessed rapid advancements in recent years, particularly in areas such as tissue repair, controlled delivery, and *in vivo* imaging. The core of this development lies in the material's ability to recognize, amplify, and programmably respond to internal and external signals [1, 2]. The realization of this series of functions essentially depends on precise "biomaterial assembly and regulation", i.e. the orderly organization of material building blocks at the molecular scale and the effective management of their dynamic behavior [3, 4].

The development of biomaterials follows an evolutionary path from "bioinertness" and "bioactivity" to "intelligent response" [5]. From the perspective of materials science, Iqbal *et al*. systematically reviewed the performance evolution of biomaterials from the initial passive

compatibility of "inertness" to the active regulation of biological environment of "activity" and pointed out that the integration of biomimetic design and dynamic behavior of "intelligent response" was its future direction [6]. Under this trend, researchers are committed to developing new intelligent response materials. Beletech *et al*. developed a hydrogel that combined decellularized tissue, verified its capability to respond to multiple physical, chemical, and biological stimuli, and demonstrated its application potential in the fields of health and ecological restoration [7]. To achieve more precise functions, Morris *et al*. constructed an antibacterial delivery system that could respond to dual stimuli of temperature and pH and realize the localized release of active substances based on Boolean logic gates, which was a manifestation of the ingenious design of intelligent response materials [8]. Among the mainstream smart responsive biomaterials, various types have been extensively studied. Weng *et al*. reviewed inorganic nanomaterials represented by ZnO and summarized their response mechanisms to single or multiple stimuli such as light and pH and their applications in biomedicine [9]. Stimulus-responsive polymers are another major research hotspot. Yadav *et al*. pointed out that these materials could be used as drug controlled-release carriers to achieve precise spatiotemporal delivery to promote tissue regeneration [10]. Roy *et al*. also focused on stimulus-responsive hydrogels/nanogels and systematically summarized their synthesis design, physicochemical property regulation, and their application value in biosensing and drug delivery [11]. In addition to soft materials, smart responsive properties have also been extended to rigid implants. Zhang *et al*. reviewed smart responsive titanium implants and pointed out that they could respond to internal and external stimuli of pathological micro-environments such as bacterial infection, achieving on-demand treatment and regeneration functions [12]. In addition, Li *et al*. reviewed stimulus-responsive self-degradable polymers (SIPs), emphasizing their unique "one stimulus, multiple responses" chemical amplifier characteristics, which demonstrated significant promise in the realms of drug delivery and molecular imaging [13]. In the field of biomedical imaging, Yang *et al*. reviewed the strategies and applications of using radionuclides to label biological carriers such as bacteria, providing a reference for related research [14]. Many researchers have systematically studied the stimulus types, structure-activity relationships, and application prospects of smart responsive biomaterials, exploring multi-stimulus coupling and integrated delivery-imaging approaches. Despite these advances, a core challenge remains in improving the "specificity" and "programmability" of biomaterial responses. Most existing response mechanisms primarily rely on non-sequence specific processes such as temperature, pH, ionic strength, or physical stimuli. Consequently, achieving a balance between selectivity, flux, and spatiotemporal precision at the molecular level is difficult.

Current research faces shortcomings including a lack of sequence-level specificity in molecular recognition, difficulty in enzymatic amplification of low-abundance signals, and limited versatility in cross-scale coupling from molecular events to macroscopic material structure. To address these limitations, this study proposed a universal platform concept centered around programmable nucleic acid recognition. A dual-function regulatory system was constructed by coupling the CRISPR-Cas12a "cis-cleavage" and "trans-cleavage" mechanisms with a DNA-functionalized polymer backbone. The cis-cleavage activity generated directional sticky ends to mediate the programmable assembly of the hydrogel, while the target-activated trans-cleavage activity triggered the degradation of the network. This design overcame sensitivity bottlenecks through enzymatic amplification and offered a modular process for cell-compatible engineering. Ultimately, this research established a new approach for the design, assembly, and dynamic regulation of intelligent biomaterials based on nucleic acid sequence logic.

Materials and methods

Expression and purification of Cas12a protein

The study constructed the pET-28a-LbCas12a plasmid in-house by cloning the codon-optimized LbCas12a gene (GenBank Accession No. WP_051666128.1) including the N-terminal His6 tag and nuclear localization signal from *E. coli* into the pET-28a(+) expression vector (Novagen, Madison, WI, USA) and then transformed it into BL21(DE3) competent cells (Novagen, Madison, WI, USA) [15]. Single positive colonies were picked and inoculated into LB medium containing 50 μg/mL kanamycin and shaken at 37°C, 220 rpm overnight. The protein was purified by using GE ÄKTA pure protein liquid chromatography system (GE Healthcare, Chicago, IL, USA).

CRISPR RNA (crRNA) design and *in vitro* transcription (IVT)

Targeting the pre-determined DNA target in the biomaterial precursor, the corresponding crRNA was designed by using a direct repeat (DR) backbone of approximately 20 nt and a spacer of 21–23 nt, which was perfectly complementary to the non-target strand downstream of the 5'-TTTV-3' protospacer adjacent motif (PAM) upstream of the target site.

In vitro activity verification of the Cas12a system

To ensure that the purified Cas12a protein and the designed crRNA possessed the expected biological activities, a series of *in vitro* activity verifications were performed. Equimolar LbCas12a and crRNA were incubated at ambient temperature for a duration of 15 min to assemble into ribonucleoproteins (RNPs). Real-time fluorescence detection was further performed by using Thermo Fisher Varioskan LUX multifunctional microplate reader (Thermo Fisher, Waltham, MA, USA) in a system containing RNP, a specific dsDNA activator, and a fluorescence-quenching labeled ssDNA probe (ssDNA-FQ). Subsequently, the cleavage reactions were performed at 37°C for 60 minutes. If the results showed that fluorescence increased rapidly only in the presence of the activator, it indicated that Cas12a trans-cleavage was triggered and the reporter probe was efficiently degraded, thereby achieving signal conversion and enzymatic amplification.

Preparation and characterization of DNA functionalized hydrogel precursors

To construct a gel network that could be recognized and cross-linked by the CRISPR system, a DNA-functionalized hydrogel precursor was prepared through a covalent coupling reaction with a biocompatible four-arm polyethylene glycol (PEG) maleimide (4-arm-PEG-Maleimide) (MW 20 kDa) (JenKem Technology, Beijing, China) as the core backbone. The backbone was dissolved in HEPES buffer at pH 7.4 followed by adding purified specific DNA oligonucleotide sequence modified with a thiol (-SH) group at the 5' end (Sangon Biotech, Shanghai, China) [16, 17]. Under room temperature and light-protected conditions, DNA strands were covalently linked to each arm of the PEG using a highly efficient and specific Michael addition reaction. The successful conjugation reaction was validated by observing the absence of the characteristic proton peak (approximately δ 6.7 ppm) on the maleimide double bond. Simultaneously, the absorbance of the product at 260 nm was estimated by using a UV-Vis spectrophotometer, and the average number of DNA strands conjugated to each PEG molecule was calculated based on the molar extinction coefficient of DNA to determine the functionalization efficiency of the precursor. The DNA primers and oligonucleotide sequences used in this study were shown in Table 1.

Hydrogel assembly experiment based on Cas12a

The experiment first verified the programmable assembly of hydrogels based on the Cas12a enzyme cleavage activity. The core principle of this strategy was to use the Cas12a/crRNA complex to specifically cut the double-stranded "bridging" DNA, thereby exposing two different sticky ends [18]. The two newly generated sticky ends hybridized with complementary sequences on the cantilever arms of two DNA-functionalized four-armed PEG precursors (PEG-A and PEG-B), thereby efficiently crosslinking the originally free

Table 1. Sequences of DNA primers and oligonucleotides.

Name	Sequence (5' to 3')	Modification
Primers	-	-
LbCas12a-Forward	CGCGGATCCATGAGCAAGCTGGAGAAG	N/A
LbCas12a-Reverse	CCGCTCGAGTTACTTTTCATCTTTGCC	N/A
Oligonucleotides	-	-
Thiol-DNA A	AAAAAAAAAAGCTAGCTG	5'-Thiol
Thiol-DNA B	AAAAAAAAAACGATCGAC	5'-Thiol
Bridging DNA (Target Strand)	GGATCTAGTTTAGCATCAAGGCTAATCATGGTCCGATCGAC	N/A
Activator DNA (Target Strand)	CGTACTGTTTAGCATCAAGGCTAATCATGGTC	N/A
crRNA	UAAUUUCUACUAAGUGUAGAUGCAUCAAGGCUAAUCAUGGUC	N/A

polymer precursor molecules to form a macroscopic hydrogel network. This assembly process exhibited a high degree of procedurality and specificity. In the control experiment lacking any component of Cas12a protein, crRNA, or bridging DNA, the system failed to gel and remained in a liquid state [19]. The process was quantitatively characterized by dynamic rheological monitoring using a DHR-2 rotational rheometer (TA Instruments, New Castle, DE, USA). To initiate the assembly, the DNA-functionalized PEG precursors were mixed with the complementary bridging DNA strands (Sangon Biotech, Shanghai, China) in HEPES buffer. The formation of the hydrogel network was monitored *in situ*. The gelation kinetics and mechanical properties were quantitatively characterized by dynamic rheological monitoring using a rotational rheometer. The time-sweep mode was employed to record the changes in storage modulus (G') and loss modulus (G'') immediately after mixing.

Hydrogel-based responsive degradation experiments based on Cas12a

To test the DNA signal-responsive degradation of the hydrogels, disc-shaped hydrogel samples prepared using a specific ssDNA crosslinking agent with 5 mm in diameter and 1 mm thick were first placed in 24-well plates and fully swollen with PBS buffer. Subsequently, solutions containing pre-assembled Cas12a/crRNA complexes at the final concentrations of 200 nM and 240 nM, respectively, were added to each hydrogel sample. The plates were incubated at 37°C for 30 min to allow the RNP complexes to fully diffuse into the gel network. The degradation reaction was triggered by adding different dsDNA trigger sequence solutions at the final concentration of 500 nM to the wells. To verify the specificity of the degradation, four experimental groups were set up including Trigger-Seq1 group with the adding of a dsDNA trigger molecule that perfectly matched crRNA, blank control group with no dsDNA trigger molecule but only equal volume of PBS, non-match seq group with the adding of a non-matching dsDNA molecule that had completely unrelated sequence, and mismatch seq group with the adding of a dsDNA molecule containing a single base mismatch. The macroscopic morphological changes during the degradation process were recorded by taking photos at regular intervals. Meanwhile, the mechanical property changes of the gel were monitored in real time using a rotational rheometer in time-scan mode. The gel sample was placed between the parallel plate clamps of the rheometer, and the test was started immediately after the trigger sequence was added. The test conditions were set to fixed strain (1%) and fixed frequency (1 Hz). The changes in storage modulus (G') and loss modulus (G'') over time were continuously monitored with the total test time of 2 hours.

Cell compatibility and drug release experiments

To evaluate the bioapplication potential of hydrogel, cytocompatibility and on-demand release experiments were performed. Human umbilical vein endothelial cells (HUVECs) were

Table 2. Analysis of in vitro cis-cutting efficiency of the Cas12a system.

Group	Cas12a (nM)	crRNA Type	crRNA (nM)	Target dsDNA	Cleavage efficiency (%)
1	50	Specific crRNA-1	60	With correct PAM	96.472 ± 2.158
2	50	None	0	With correct PAM	1.839 ± 0.521
3	50	Mismatch crRNA-2	60	With correct PAM	3.216 ± 0.745
4	0	Specific crRNA-1	60	With correct PAM	0.000 ± 0.000
5	50	Specific crRNA-1	60	PAM-less	4.081 ± 0.882

employed in this study. Logarithmic-phase cells were digested and counted, then mixed at approximately 2 × 10^6 cells/mL with two DNA-functionalized PEG precursors and a bridging DNA. Cas12a–crRNA was added to initiate *in situ* crosslinking, and the cells were incubated in a microfluidic chamber or PDMS mold at 37°C and 5% CO_2 for 1 hour to form a three-dimensional encapsulation. A Calcein-AM/PI double staining kit was employed, and z-axis imaging was obtained through a Leica TCS SP8 laser scanning confocal microscope (Leica, Wetzlar, Germany) to assess the viability and morphology of the three-dimensional network on days 1, 3, and 5 after encapsulation. A model drug release assay was performed by using a drug-loaded hydrogel co-encapsulated with FITC-Dextran. Experimental groups with and without the specific DNA trigger were set up. The cumulative release rate was calculated by periodically monitoring the fluorescence intensity of the release solution to characterize the on-demand release performance of the system.

Statistical analysis

All quantitative experiments underwent independent repetition for a minimum of three times. The experimental data were presented as mean ± standard deviation (SD). Statistical analysis and graph generation were performed by using GraphPad Prism 9 software (https://www.graphpad.com). Two-tailed Student's t-test was performed to compare the means between two groups [20], while one-way ANOVA was used for the comparison of the means of three or more groups combined with Tukey's post-hoc test for pairwise significance analysis. *P* value less than 0.05 was defined as statistically significant.

Results and discussion

Preparation and activity characterization of Cas12a protein

The study precisely quantified the targeted cleavage (cis) activity of the purified LbCas12a protein. To verify that its activity depended not only on the presence of crRNA but also on the correct target sequence and PAM motif, the study designed multiple control groups including those with a complete system, those lacking key components, or those with sequence errors. The analysis results of the *in vitro* cis-cleavage efficiency of the Cas12a system showed that, in the presence of 50 nM Cas12a and 60 nM crRNA-1, the cleavage efficiency for the correct target (Group 1) reached a saturation level of 96.472 ± 2.158%. In contrast, the cleavage efficiency was negligible when crRNA was absent (Group 2) or when non-matching crRNA-2 was used (Group 3) at 1.839 ± 0.521% and 3.216% ± 0.745%, respectively. Crucially, when the target dsDNA lacked the correct PAM sequence (Group 5), even with all other conditions met, the cleavage efficiency was only 4.081 ± 0.882% (Table 2). The Cas12a trans-cleavage activity demonstrated that the fluorescence signal of the complete system was weak in the initial phase of the reaction, then increased fast in an S-shaped curve, and finally reached a saturation plateau at a high level of about 120,000 random units. In contrast, the control group lacking activators or using mismatched activators maintained a very low background level throughout the monitoring time without significant increase (Figure 1a). The relationship between the initial reaction rate and the activator concentration showed that the initial reaction rate increased with the increase of activator concentration and increased rapidly in

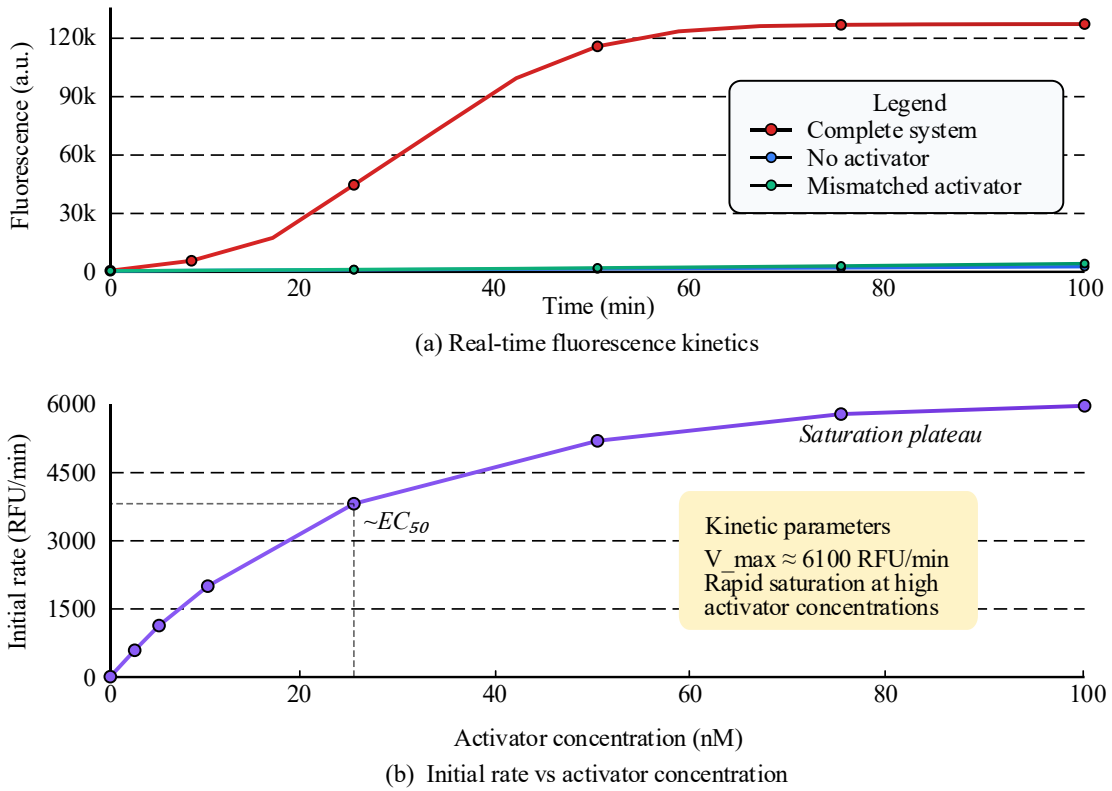

Figure 1. Characterization of Cas12a trans-cleavage activity.

the low concentration range, then slowed down, and gradually approached a saturation plateau at high concentrations. The maximum reaction rate was about 6,100 RFU/min, and the activator concentration (EC_{50}) at which the reaction reached half maximum rate was then determined (Figure 1b).

CRISPR - Cas12a - mediated programmable assembly of hydrogels

The study further explored the influence of key component concentrations on the macroscopic physical properties of the hydrogels. By manipulating the total concentration of the polymer precursor (DNA-functionalized PEG), which served as the basis for the cross-linked network, the effect on gelation kinetics and ultimate mechanical strength was studied. The results showed that, as the polymer concentration increased from 2.5% to 7.5%, the gelation time (the intersection of G' and G'') decreased dramatically from 41.37 minutes to 15.19 minutes. More significantly, the final gel hardness (G' value at 60 minutes) increased nearly threefold from 788.163 ± 45.312 Pa to 2,864.308 ± 152.994 Pa. Concomitantly, the G'/G'' ratio increased significantly from 16.8 to 42.3, indicating that higher polymer concentrations formed a more densely cross-linked, elastic solid network. The slight difference in initial complex viscosity (at t = 0) also reflected the different initial concentrations of the precursor solutions (Table 3). The rheological properties of the hydrogel assemblies demonstrated that the storage modulus (G') of the experimental group increased rapidly over time and surpasses the loss modulus (G'') at about 15 minutes, which was the gel point. Subsequently, G' continued to rise sharply and eventually reached a plateau at a level exceeding 1,000 Pa, indicating that the system successfully transformed from a liquid state (G'' > G') to a gel state (G' > G''). In contrast, the G' and G'' of the control group remained at extremely low levels

Table 3. Effect of different polymer concentrations on the physical properties of hydrogels.

Experiment ID	Polymer conc. (w/v %)	Initial complex viscosity (Pa·s) at t = 0	Gelation time (min)	Final storage modulus G' (Pa) at 60 min	Final loss modulus G'' (Pa) at 60 min	Final G'/G'' ratio
H-2.5	2.50%	0.018 ± 0.003	41.37	788.163 ± 45.312	46.882 ± 4.109	16.8
H-5.0	5.00%	0.031 ± 0.004	24.82	1,512.791 ± 88.245	43.881 ± 3.576	34.5
H-7.5	7.50%	0.054 ± 0.006	15.19	2,864.308 ± 152.994	67.763 ± 5.922	42.3

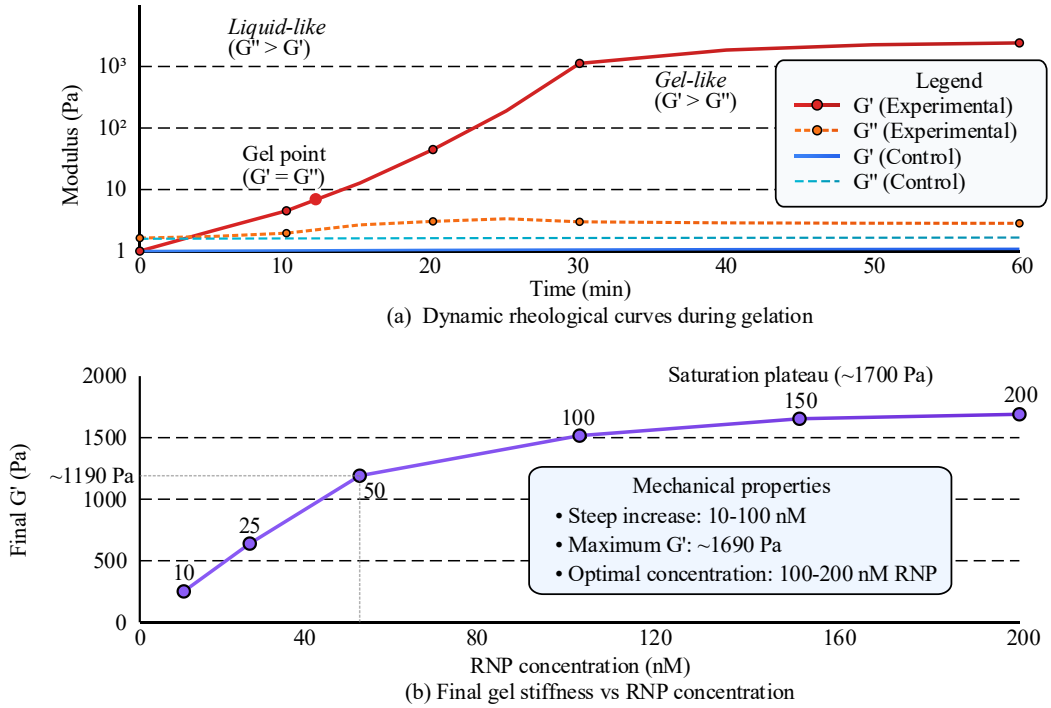

Figure 2. Rheological properties of hydrogel assembly.

throughout the process and did not cross over, and the system remained in a liquid state (Figure 2a). By further exploring the relationship between the final gel hardness (Final G') and the concentration of the RNP complex, the results revealed that the final hardness of the gel exhibited a positive correlation with the escalating RNP concentration, especially in the concentration range of 10 to 100 nM. When the concentration continued to increase, the increase in hardness gradually slowed down and eventually reached a saturation plateau at about 1,700 Pa, indicating that the mechanical properties of the gel could be effectively controlled by adjusting the RNP concentration (Figure 2b).

Dynamic regulation of DNA signal responsiveness of hydrogels

To rigorously validate the sequence-specificity of the hydrogel degradation process for DNA signaling molecules, the changes in mechanical properties during the degradation process and the final state were quantified. The quantitative analysis of the effects of different DNA trigger sequences on hydrogel degradation with the gels loaded with 150 nM RNP complexes showed that the gel underwent effective degradation with its

Table 4. Quantitative analysis of hydrogel degradation induced by different DNA trigger sequences.

Group	Trigger sequence (200 nM)	Initial G' (Pa)	G' at 1h (Pa)	Final G' at 2h (Pa)	G' Attenuation rate (%)	Macroscopic state after 2h
1	Trigger-Seq1	1,853.461 ± 98.172	189.554 ± 25.431	59.088 ± 11.218	96.814	Dissolved
2	None	1,861.918 ± 102.441	1,845.337 ± 101.982	1,827.643 ± 99.854	1.841	Solid
3	Non-match Seq	1,842.274 ± 95.883	1,811.029 ± 94.771	1,792.833 ± 93.916	2.684	Solid
4	Mismatch seq	1,851.092 ± 105.126	1,802.784 ± 108.313	1,769.442 ± 110.829	4.411	Solid

Table 5. Quantitative survival analysis of HUVECs cells cultured in three-dimensional hydrogels.

Culture condition	No. of images analyzed	Day 1 viability (%)	Day 3 viability (%)	Day 5 viability (%)
3D hydrogel encapsulation	5	97.619 ± 1.582	95.284 ± 1.933	92.837 ± 2.411
2D culture plate (Control)	5	98.942 ± 0.873	97.811 ± 1.229	96.559 ± 1.488
Hydrogel leachate (toxicity control)	5	98.538 ± 1.014	97.582 ± 1.301	96.124 ± 1.673

storage modulus G' dropping sharply to 189.554 Pa within 1 hour and completely dissolved after 2 hours, resulting in a G' decay rate as high as 96.814% only after the addition of a perfectly matched trigger-seq1 (Group 1). In contrast, regardless of whether the trigger molecule was absent (Group 2), a non-matching sequence was used (Group 3), or a mismatched sequence with a single base mismatch was introduced (Group 4), the G' decay rate within 2 hours was less than 5%, and the gel remained macroscopically stable in a solid state (Table 4).

Assessment of the system's biological application potential

To quantitatively assess the biocompatibility of the CRISPR-assembled hydrogels, the survival of HUVECs encapsulated within them was monitored for 5 days and compared with two control methods including traditional 2D culture and immersion solution culture. Quantitative survival analysis of HUVECs cultured in 3D hydrogels demonstrated that cells directly encapsulated in the hydrogel for 3D culture had a high survival rate of 97.619 ± 1.582% on day 1, which was not significantly different from the 2D culture plate control group (98.942 ± 0.873%). After 5 days of culture, the cell survival rate in the 3D culture group remained high at 92.837 ± 2.411%. Furthermore, the survival rate of cells cultured in the gel extract was similar to that of the 2D control group, revealing that neither the gel material itself nor any trace components released by it were significantly cytotoxic, demonstrating the excellent biocompatibility of this system (Table 5). This research successfully developed a programmable dual-functional hydrogel platform based on the CRISPR-Cas12a system. By leveraging the specific cis- and trans-cleavage activities of Cas12a, the precise regulation of hydrogel assembly and degradation was achieved at the nucleic acid sequence level. The constructed hydrogel exhibited rapid gelation, tunable mechanical properties, and excellent cytocompatibility. Furthermore, the system demonstrated exceptional specificity, enabling rapid disintegration only in the presence of perfectly matched DNA activators while maintaining stability with mismatched sequences. This study successfully extended the molecular recognition capabilities of CRISPR-Cas systems to the macroscopic regulation of soft matter, providing a versatile strategy for the development of intelligent, sequence-responsive biomaterials for biomedical applications.

References

1. Zhou J, Liu G, Zhao Y, Zhang R, Tang X, Li L, *et al*. 2023. An efficient CRISPR–Cas12a promoter editing system for crop improvement. Nat Plants. 9(4):588–604.
2. Rahimnejad M, Jahangiri S, Zirak Hassan Kiadeh S, Rezvaninejad S, Ahmadi Z, Ahmadi S, *et al*. 2024. Stimuli-responsive

biomaterials: Smart avenue toward 4D bioprinting. Crit Rev Biotechnol. 44(5):860-891.
3. Yi W, Khalid A, Arshad N, Asghar MS, Irshad MS, Wang X, *et al*. 2023. Recent progress and perspective of an evolving carbon family from 0D to 3D: Synthesis, biomedical applications, and potential challenges. ACS Appl Bio Mater. 6(6):2043-2088.
4. Chauhan A, Saini A, Sharma D. 2025. The evolution of integrated magnetic hyperthermia and chemodynamic therapy for combating cancer: A comprehensive viewpoint. Nanoscale Adv. 7(16):4820-4836.
5. Li M, Yin S, Lin M, Chen X, Pan Y, Peng Y, *et al*. 2022. Current status and prospects of metal–organic frameworks for bone therapy and bone repair. J Mater Chem B. 10(27):5105-5128.
6. Iqbal S, Sohail M, Fang S, Ding J, Shen L, Chen M, *et al*. 2023. Biomaterials evolution: From inert to instructive. Biomater Sci. 11(18):6109-6115.
7. Beletech A, Reta BK, Tesfaye T. 2025. Smart and intelligent biomaterials for novel applications–a review. Int J Polym Mater Polym Biomater. 74(2):140-158.
8. Morris G, Goodman S, Sorzabal Bellido I, Milanese C, Girella A, Pallavicini P, *et al*. 2023. Temperature and pH stimuli-responsive system delivers location-specific antimicrobial activity with natural products. ACS Appl Bio Mater. 7(1):131-143.
9. Weng Z, Xu Y, Gao J, Wang X. 2023. Research progress of stimuli-responsive ZnO-based nanomaterials in biomedical applications. Biomater Sci. 11(1):76-95.
10. Yadav D, Sharma PK, Malviya R, Mishra PS, Surendra AV, Rao GK, *et al*. 2024. Stimuli-responsive biomaterials for tissue engineering applications. Curr Pharm Biotechnol. 25(8):981-999.
11. Roy A, Manna K, Pal S. 2022. Recent advances in various stimuli-responsive hydrogels: From synthetic designs to emerging healthcare applications. Mater Chem Front. 6(17):2338-2385.
12. Zhang J, Zhuang Y, Sheng R, Tomás H, Rodrigues J, Yuan G, *et al*. 2024. Smart stimuli-responsive strategies for titanium implant functionalization in bone regeneration and therapeutics. Mater Horiz. 11(1):12-36.
13. Li Y, Liu J, He J, Dey A, Bui VD, Park JH. 2024. Recent advances in stimuli-responsive self-immolative polymers for drug delivery and molecular imaging. Chem Mater. 36(9):4054-4077.
14. Yang Y, Wang J, Zhong Y, Tian M, Zhang H. 2025. Advances in radionuclide-labeled biological carriers for tumor imaging and treatment. ACS Appl Mater Interfaces. 17(3):4316-4336.
15. Ikhazuagbe IH, Ofoka EA, Odofin OL, Erumiseli O, Edoka OE, Ezennubia KP, *et al*. 2025. Antibacterial activity and mechanistic insights of gallium-based nanoparticles: An emerging frontier in metal-based antimicrobials. RSC Adv. 15(38):31122-31153.
16. Srivastava N, Choudhury AR. 2022. Stimuli-responsive polysaccharide-based smart hydrogels and their emerging applications. Ind Eng Chem Res. 62(2):841-866.
17. Ma G, Wang K, Pang X, Xu S, Gao Y, Liang Y, *et al*. 2023. Self-assembled nanomaterials for ferroptosis-based cancer theranostics. Biomater Sci. 11(6):1962-1980.
18. Hang Y, Wang A, Wu N. 2024. Plasmonic silver and gold nanoparticles: Shape- and structure-modulated plasmonic functionality for point-of-caring sensing, bio-imaging and medical therapy. Chem Soc Rev. 53(6):2932-2971.
19. Liu J, Liu J, Mu W, Ma Q, Zhai X, Jin B, *et al*. 2024. Delivery strategy to enhance the therapeutic efficacy of liver fibrosis *via* nanoparticle drug delivery systems. ACS Nano. 18(32):20861-20885.
20. Hu Y, Chen Y, Tang H, Zhang G, Ma M, Pan Z, *et al*. 2025. Precision synthesis strategies and emerging applications of bioorthogonal click chemistry in tissue engineering and regenerative medicine. MedMat. 2(1):33-54.